applied optics

Liquid crystal microlens arrays recorded by polarization holography

Ulises Ruiz,[1,*] Pasquale Pagliusi,[2,3] Clementina Provenzano,[2] Eugenia Lepera,[2] and Gabriella Cipparrone[2,3]

[1]Instituto Nacional de Astrofísica, Óptica y Electrónica, Puebla 72000, Mexico
[2]Dipartimento di Fisica, Università Della Calabria, 87036 Rende (CS), Italy
[3]IPCF-CNR, UOS Cosenza, and Excellence Centre CEMIF.CAL, 87036 Rende (CS), Italy
*Corresponding author: uruiz@inaoep.mx

Received 12 December 2014; revised 26 February 2015; accepted 9 March 2015; posted 10 March 2015 (Doc. ID 229270); published 8 April 2015

We report the characterization of diffractive microlens arrays (MAs) using a polarization holographic approach assisted by a spatial light modulator (SLM), in a nematic liquid crystal (NLC) cell. The MAs were recorded in the photoaligning substrates of the cell and then replicated in the NLC bulk, through the surface interactions. The transparency of the NLC on a wide range of wavelengths and the ability to tune its optical birefringence, through an external voltage, allowed us to create MAs with high efficiency. We have presented the results obtained for diverse MAs configurations, composed by spherical and cylindrical microlenses and characterized by different focal lengths. The efficiency reaches a value of 90%, at a wavelength of 633 nm.

OCIS codes: (160.3710) Liquid crystals; (230.6120) Spatial light modulators; (090.1760) Computer holography; (090.2900) Optical storage materials; (210.4770) Optical recording; (260.1440) Birefringence.

http://dx.doi.org/10.1364/AO.54.003303

1. INTRODUCTION

Advancements in optical and photonic microdevices has led to extensive investigation in the last decade of the design of microcomponents, such as microlens arrays (MAs). MAs are useful for numerous applications, such as three-dimensional (3D) imaging [1,2], optical communications [3], Shack–Hartmann wavefront test [4], lab-on-chip systems [5], optofluidic devices [6], and image processing [7], among others. Several techniques to fabricate MAs have been developed, the most common being modeling the relief's shape. MAs have been created in diverse materials, such as amorphous calcium by means of self-assembling [8], borosilicate glass through local melting with a focused laser beam [9], and on liquid crystal (LC) using lithography [10,11]. LC has been extensively employed for MAs [12,13], with accordable focal length [14,15], owing to its tunable effective linear birefringence over a wide wavelength range. Thanks to this important property, LC MAs with planar geometries have been produced through the gradient index refraction (GRIN) modulation [16]. Recent studies have shown that GRIN can be created in birefringent materials through polarization holography [17,18].

The polarization holography relies on the interference of orthogonally polarized waves, where a modulation of the polarization state of the light occurs in the superposition region, as a function of the phase difference between the beams [19]. The polarization holograms (PHs) possess peculiar diffraction properties. Particularly interesting are the PHs produced by two orthogonal circular (left and right) polarizations in polarization sensitive materials, where only the zero (0) and the first (± 1) diffracted orders appear, with the left (or right) circularly polarized $+1$ (-1) order proportional to the right- (left-) hand component of the incident wave. Moreover, 100% diffraction efficiency can be achieved for proper values of the optical retardance [19]. Different from the techniques mentioned above, polarization holography is a direct recording technique, which offers important advantages, such as a short writing time, low recording intensity, and stable systems. In this sense, it is possible to create MAs on a thin plane sample and control independently the GRIN geometry of each microlens (i.e., spherical, aspherical, cylindrical microlenses, or combinations of them).

Here we report a method to generate highly efficient and electrically controllable diffractive MAs, which facilitates encoding the parameters of each microlens. The phase information of the MAs is stored in a nematic LC (NLC) cell by using a polarization holographic approach assisted by spatial light modulator (SLM), which creates the two orthogonally polarized fields to construct the PH. Exploiting the transparency of the LC over a wide wavelength range and the spatially inhomogeneous linear birefringence, obtained by recording the PH on the photosensitive aligning substrates, diverse combinations of MAs including spherical and cylindrical microlenses have

been created, controlling their GRIN. In particular, our MAs have potential applications in biophotonics [20], fiber coupling [21], patterning by flood illumination [22], and solar cells [23]. In addition, unlike the MAs obtained by direct recording on photobirefringent polymer [18], by applying a small voltage to the NLC cell, the MAs diffraction efficiency can be optimized for the spectral range of interest. Here we have demonstrated an efficiency of 90% at 633 nm.

2. THEORY

The MAs are codified using a PH, which is created by the interference between a plane wave and the phase element corresponding to the MAs, having orthogonal circular polarizations and whose propagation axes form a small angle θ. The interfering fields can be written as

$$\vec{E}_P = \frac{1}{\sqrt{2}}\begin{pmatrix}1\\ i\end{pmatrix}e^{i\delta}, \qquad \vec{E}_L = \frac{1}{\sqrt{2}}\begin{pmatrix}1\\ -i\end{pmatrix}e^{i\psi(x,y)}e^{-i\delta}, \tag{1}$$

where $\delta = \frac{\pi}{\Lambda}x$, with $\Lambda = \frac{\lambda_R}{2\sin(\theta/2)}$ representing the spatial period of the polarization pattern, λ_R is the recording wavelength, and $\psi(x,y) = \sum_{n=1}^{N}\sum_{m=1}^{M}\psi_{nm}(x,y)$ is the phase of the $N \times M$ MA. The phase of each microlens in $\psi(x,y)$ can be expressed by

$$\psi_{nm} = \pi(a_{nm}(x - x_{nm})^2 + b_{nm}(y - y_{nm})^2)/(\lambda_R f_{nm}), \tag{2}$$

where a_{nm}, b_{nm} are constant values in the range [0,1], (x_{nm}, y_{nm}), f_{nm} are the center coordinates and the focal distance of each microlens, respectively. For simplicity, we have omitted the (x,y) dependence in the phase function ψ. The resulting optical field pattern in the superposition region is

$$\vec{E}_{\text{tot}} = \vec{E}_P + \vec{E}_L = \frac{1}{\sqrt{2}}\begin{pmatrix}e^{i\delta} + e^{i\psi}e^{-i\delta}\\ ie^{i\delta} - ie^{i\psi}e^{-i\delta}\end{pmatrix}. \tag{3}$$

The Stokes parameters of this field can be expressed by [19] $S_0 = 1$, $S_1 = 2\cos(2\delta - \psi)$, $S_2 = 2\sin(2\delta - \psi)$, $S_3 = 0$, and the transmission matrix of the recorded hologram is

$$L = \begin{bmatrix}\cos M + ikd\gamma_{\text{lin}}S_1\frac{\sin M}{M} & ikd\gamma_{\text{lin}}S_2\frac{\sin M}{M}\\ ikd\gamma_{\text{lin}}S_2\frac{\sin M}{M} & \cos M - ikd\gamma_{\text{lin}}S_1\frac{\sin M}{M}\end{bmatrix}, \tag{4}$$

where $M = kd\sqrt{\gamma_{\text{lin}}^2(S_1^2 + S_2^2)}$, k is the wavenumber, d is the thickness of the film, γ_{lin} is a coefficient related to the effective linear birefringence. By substituting the Stokes parameters into Eq. (4), we evaluate the transmission matrix of the hologram, which can be written as sum of the three matrices associated with the 0 and the ± 1 diffraction orders:

$$\begin{aligned}L = L_0 + L_{+1} + L_{-1} &= \begin{bmatrix}1 & 0\\ 0 & 1\end{bmatrix}\cos(2kd\gamma_{\text{lin}})\\ &+ \frac{1}{2}\begin{bmatrix}i & -1\\ -1 & -i\end{bmatrix}\sin(2kd\gamma_{\text{lin}})e^{-i\psi}\\ &+ \frac{1}{2}\begin{bmatrix}i & 1\\ 1 & -i\end{bmatrix}\sin(2kd\gamma_{\text{lin}})e^{i\psi}.\end{aligned} \tag{5}$$

The $+1$ and -1 orders in Eq. (5) have conjugated phases, meaning that it is possible to get a MA with positive focal length on a diffracted order and negative focal length on the other.

3. EXPERIMENTAL RESULTS

Here we employed a synthetic phase hologram (SPH) [24], displayed on a SLM, to produce the PH. This SPH is characterized by a linear carrier grating, which puts off-axis its diffraction orders and avoids the on-axis noise due mainly to the unmodulated reflected light, on the air–glass interface of the SLM. We exploited the proved capabilities of the SPH, to generate arbitrary complex fields, to simultaneously create the plane wave and the MAs needed for the PH. However, because of the pixelated structure of the SLM, a modulation envelope function influences the amplitude distribution of the fields; thus we applied a digital prefiltering to compensate for this effect [25,26].

Figure 1 shows the experimental setup used to record the MA holograms. An expanded Argon laser beam ($\lambda_R = 488$ nm) impinges over a phase-only SLM (Holoeye–PLUTO), which generates two s-polarized fields (i.e., the MAs and the plane wave). The lens L_1 projects the Fourier spectrum of the SPH on its focal plane. The SPH presents several noise orders; therefore, a binary spatial filter (SF) is employed to block the high diffraction orders produced by the pixelated structure of the SLM and to transmit only the $+1$-diffraction order of the SPH. Therefore, the spectra of the plane wave and the MAs are transmitted. For simplicity, in the experimental setup, we only depicted three diffraction orders that correspond to the on-axis order, the plane wave and the MAs. The s-polarization of the plane wave field is converted in p-polarization by means of a half-wave plate (HWP), to obtain orthogonal linear polarizations. Finally, a second lens L2 recovers and projects the beams on the sample (S) and a quarter-wave plate (QWP) converts the orthogonal linear polarizations of the fields to opposed circular polarizations. The lenses employed (L_1, L_2) have a focal length of $f = 300$ mm, the interference angle between the fields is $\theta \approx 0.5°$.

We have experimentally investigated the codification of MAs in a 2 μm thick NLC layer, confined between two conductive ITO glass plates, coated by 10 nm thick photoaligning azobenzene material [27], as shown in Fig. 2. When the latter

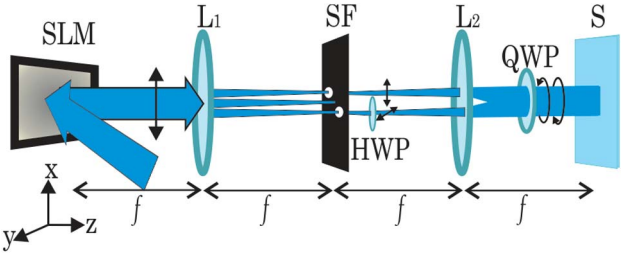

Fig. 1. Experimental setup used to record the PH. A linearly polarized argon laser ($\lambda_R = 488$ nm) impinges over a SLM, which displays a SPH to generate a plane wave and the phase element corresponding to the MA. The lens L_1 realizes the Fourier transform of the SPH so a binary spatial filter (SF) is placed in the focal plane that blocks the zeroth order of the SPH. The (HWP) rotates by 90° the linear polarization of the plane wave. The lens L_2 collects and projects an image of the two interfering fields, which generate the PH, on the sample (S). The orthogonal linear polarizations are transformed to circular opposed polarizations by means of the (QWP).

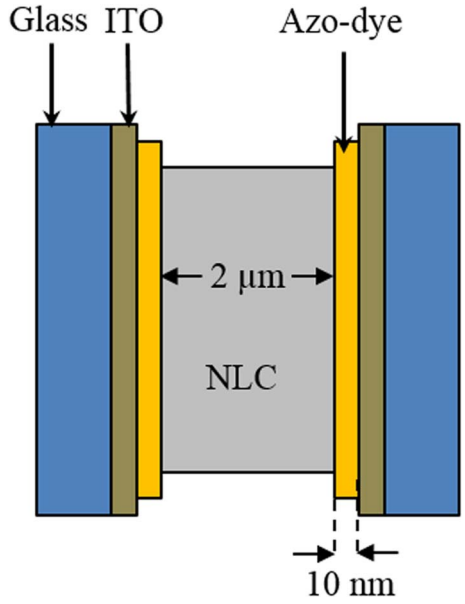

Fig. 2. Scheme of the cell. A 2 μm thick NLC layer is confined between two conductive ITO glass plates, coated by 10 nm thick photoaligning azobenzene material.

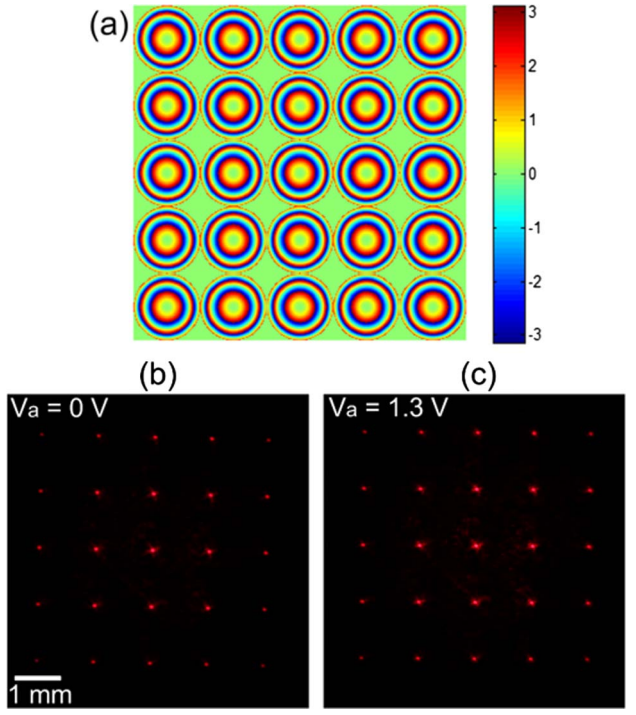

Fig. 3. 5 × 5 MA, (a) phase distribution of the MA, which is composed by 25 spherical microlenses ($f_{\text{sph}} = 2.5$ cm). The intensity of the He–Ne probe beam is recorded 2.5 cm behind the PH, where the spherical microlenses are focused, without (b) and with (c) the applied voltage ($V_a = 1.3$ V).

are exposed to the interference field in Eq. (3), the azobenzene molecules reorient according to the direction of the local linear polarization of the field, thus providing spatially modulated planar anchoring for the LC layer. Afterward, the empty cell is filled with the NLC mixture E7 (BL001, Merck) in the isotropic phase at 65°C and slowly cooled down to room temperature. In the nematic phase, this NLC has a birefringence of 0.22 for $\lambda = 633$ nm.

The PH recorded on the two command azobenzene films are replicated in the NLC layer, where the phase information of the MAs is stored. Several phase configurations have been designed to create MAs including spherical and cylindrical microlenses with different focal lengths. The total recording intensity and the exposure time are 50 mW/cm^2 and 120 s, respectively. A circularly polarized He–Ne laser probe beam ($\lambda_P = 633$ nm), whose wavelength is far from the absorption band of the azobenzene photoaligning material, has been used to analyze the features of the MAs, in the −1 diffracted order. The diffraction efficiency measured for the MA holograms is 78%. Nevertheless, a weak voltage applied to the ITO substrates allows modification of the effective linear birefringence of the NLC layer, and wide adjustment of the diffraction efficiency in the spectral range of interest, through γ_{lin} [28].

A 5 × 5 MA is shown in Fig. 3, which is composed by spherical microlenses ($a_{nm} = b_{nm} = 1$), each one with a diameter of $D \approx 1.28$ mm and focal length 2.5 cm. The effective focal length depends on the recording (λ_R) and probe (λ_P) wavelengths as $f^P_{nm} = \lambda_R f_{nm}/\lambda_P = 0.77 f_{nm}$. Figure 3(a) shows the phase distribution that corresponds to the MA, which focalizes 2.5 cm behind the PH, whereas the −1 diffracted order of MA with applied RMS voltage $V_a = 0$ V and $V_a = 1.3$ V is shown in Figs. 3(b) and 3(c), respectively. It is evident from Figs. 3(b) and 3(c) that the diffraction efficiency increases when the proper voltage is applied, namely from 78% at $V_a = 0$ V to 90% at $V_a = 1.3$ V.

Figure 4(a) shows a second mixed 4 × 4 MA, where each microlens has a diameter $D \approx 1.6$ mm, composed by 12 spherical microlenses ($a_{1j} = b_{1j} = a_{4j} = b_{4j} = a_{21} = b_{21} = a_{24} = b_{24} = a_{31} = b_{34} = 1$ with $j = 1, 2, 3, 4$) with focal length $f_{\text{sph}} = 5$ cm, 2 horizontal ($a_{22} = a_{33} = 1$, $b_{22} = b_{33} = 0$) and 2 vertical ($a_{23} = a_{32} = 0$, $b_{23} = b_{32} = 1$) cylindrical microlenses with focal length $f_{\text{cyl}} = 10$ cm. Figures 4(b) and 4(c) show the transmitted intensity of the probe beam recorded 5 cm behind the PH, where the spherical microlenses are focused, with applied voltage $V_a = 0$ V and $V_a = 1.3$ V, respectively. The transmitted intensity recorded 10 cm behind the PH, where the cylindrical microlenses are focused, with applied voltage $V_a = 0$ V and $V_a = 1.3$ V, is shown in Figs. 4(d) and 4(e), respectively. This applied RMS voltage maximizes the efficiency of the MAs for the probe wavelength; however, it can be tuned to maximize the efficiency in the whole visible range [29].

The weak background noise, which can be seen in Figs. 3(b) and 3(c), can be attributed to the fact that the microlenses are defined on a circular pupil [Fig. 3(a)]. There are, indeed, regions of the command films, corresponding to the dark area in the interference field of Eq. (3) between the microlenses, that do not provide a definite anchoring and then the inhomogeneous NLC layer in these regions scatters the impinging light.

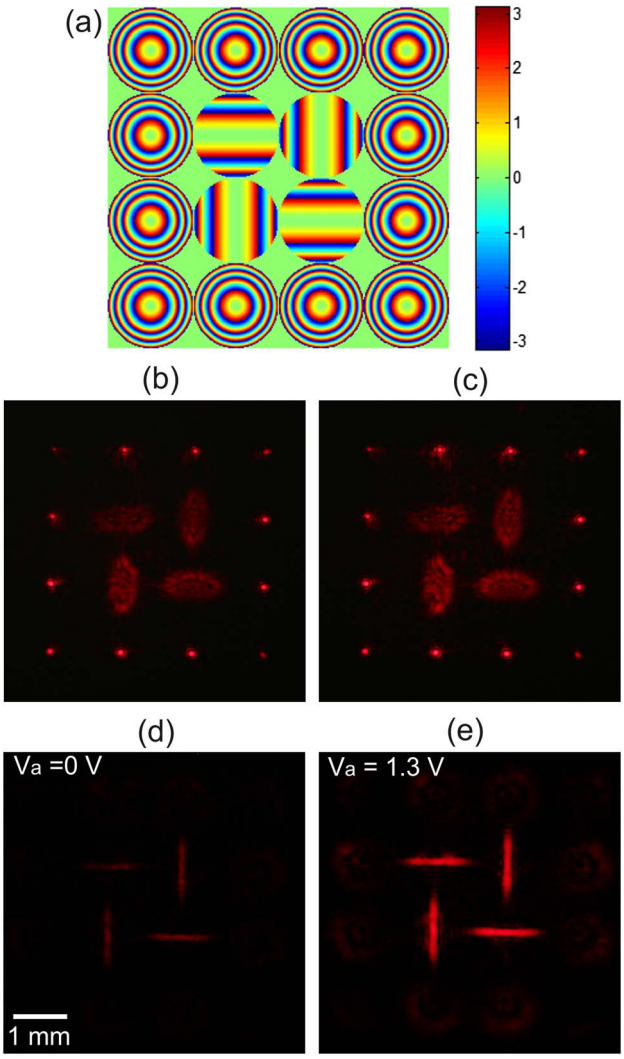

Fig. 4. 4×4 mixed MA, which is composed by 12 spherical microlenses ($f_{\text{sph}} = 5$ cm), 2 horizontal and 2 vertical cylindrical microlenses ($f_{\text{cyl}} = 10$ cm). The intensity of the probe beam is recorded 5 cm behind the PH where the 12 spherical microlenses are focused, without (b) and with (c) applied voltage ($V_a = 1.3$ V). The probe beam intensity is recorded 10 cm behind the PH where the cylindrical microlenses are focused, without (d) and with (e) applied voltage ($V_a = 1.3$ V).

4. CONCLUSIONS

We have presented an all-optical technique to create electrically tunable and highly efficient diffractive MAs based on SLM-assisted polarization holography. This method allowed us to design a GRIN on a thin LC cell to create different MAs configurations. By changing the circular polarization handedness of the probe beam, the MAs can be switched between positive and negative focal length over the two ± 1 diffracted orders, as it was reported in a previous work [18]. A feature with respect to [18] is that the controllable linear birefringence, through an applied voltage, and the transparency of the LC helps to maximize the diffraction efficiency close to 100%, in the whole visible range. We have shown two MAs configurations characterized by spherical and cylindrical microlenses with different focal lengths that are in good agreement with the focalization properties of these types of elements. By applying a weak voltage ($V_a = 1.3$ V) to the NLC cell, we have reported a total efficiency of the MAs of 90%, at the wavelength of the He–Ne probe beam ($\lambda_P = 633$ nm). Additionally, the robustness of the proposed method can be exploited to generate bigger mixed MAs by combining it with a two-dimensional (2D) displacement system.

Ulises Ruiz acknowledges support from Consejo Nacional de Ciencia y Tecnología (CONACYT) México.

REFERENCES

1. S. Dong-Hak, L. Byoungho, and K. Eun-Soo, "Improved viewing quality of 3D images in computational integral imaging reconstruction based on lenslet array model," ETRI J. **28**, 521–524 (2006).
2. Y. P. Huang, C. W. Chen, T. C. Shen, and J. F. Huang, "Autostereoscopic 3D display with scanning multi-electrode driven liquid crystal (MeD-LC) lens," J. 3D Res. **1**, 39–42 (2010).
3. W. Pan, L. Liu, H. Liu, and S. Deng, "A novel technique for wireless optical communications with lenslet array processor," Chin. Opt. Lett. **4**, 265–267 (2006).
4. M. Ares, S. Royo, and J. Caum, "Shack–Hartmann sensor based on a cylindrical microlens array," Opt. Lett. **32**, 769–771 (2007).
5. P. Fei, Z. He, C. Zheng, T. Chen, Y. Men, and Y. Huang, "Discretely tunable optofluidic compound microlenses," Lab Chip **11**, 2835 (2011).
6. J. C. Roulet, R. Volkel, H. P. Herzig, E. Verpoorte, N. F. de Rooij, and R. Dandliker, "Fabrication of multilayer systems combining microfluidic and microoptical elements for fluorescence detection," J. Microelectromech. S. **10**, 482–491 (2001).
7. Y. J. Lee, J. H. Baek, Y. Kim, J. U. Heo, Y. K. Moon, J. S. Gwag, C. J. Yu, and J. H. Kim, "Polarizer-free liquid crystal display with electrically switchable microlens array," Opt. Express **21**, 129–134 (2013).
8. K. Lee, W. Wagermaier, A. Masic, K. P. Kommareddy, M. Bennet, I. Manjubala, S. Lee, S. B. Park, H. Cölfen, and P. Fratzl, "Self-assembly of amorphous calcium carbonate microlens arrays," Nat. Commun. **3**, 1–8 (2012).
9. M. Fritze, M. B. Stern, and P. W. Wyatt, "Laser-fabricated glass microlens arrays," Opt. Lett. **23**, 141–143 (1998).
10. M. H. Wu, C. Park, and G. M. Whitesides, "Fabrication of arrays of microlenses with controlled profiles using gray-scale microlens projection photolithography," Langmuir **18**, 9312–9318 (2002).
11. L. G. Commander, D. E. Day, and D. R. Selviah, "Variable focal length microlenses," Opt. Commun. **177**, 157–170 (2000).
12. H. Ren, Y. H. Fan, and S. T. Wu, "Liquid-crystal microlens arrays using patterned polymer networks," Opt. Lett. **29**, 1608–1610 (2004).
13. M. Xu, Z. Zhou, H. Ren, S. H. Lee, and Q. Wang, "A microlens array based on polymer network liquid crystal," Appl. Phys. Lett. **113**, 053105 (2013).
14. Y. Choi, J. H. Park, J. H. Kim, and S.-D. Lee, "Fabrication of a focal length variable microlens array based on a nematic liquid crystal," Opt. Mater. **21**, 643–646 (2002).
15. H. T. Dai, Y. J. Liu, X. W. Sun, and D. Luo, "A negative-positive tunable liquid-crystal microlens array by printing," Opt. Express **17**, 4317 (2009).
16. T. Nose and S. Sato, "A liquid crystal microlens obtained with a non-uniform electric field," Liq. Cryst. **5**, 1425 (1989).
17. P. S. Ramanujam, C. Dam-Hansen, R. H. Berg, S. Hvilsted, and L. Nikolova, "Polarization-sensitive optical elements in azobenzene polyesters and peptides," Optics and Lasers in Engineering **44**, 912–925 (2006).
18. U. Ruiz, C. Provenzano, P. Pagliusi, and G. Cipparrone, "Single-step polarization holographic method for programmable microlens arrays," Opt. Lett. **37**, 4958–4960 (2012).
19. L. Nikolova and P. S. Ramanujam, *Polarization Holography* (Cambridge University, 2009).

20. J. Kuo, C. Hsieh, S. Yang, and G. Lee, "An SU-8 microlens array fabricated by soft replica molding for cell counting applications," J. Micromech. Microeng. **17**, 693 (2007).
21. J. Y. Hu, C. P. Lin, S. Y. Hung, H. Yang, and C. K. Chao, "Semi-ellipsoid microlens simulation and fabrication for enhancing optical fiber coupling efficiency," Sens.Actuators A Phys. **147**, 93 (2008).
22. M. Wu, K. Paul, and G. Whitesides, "Patterning flood illumination with microlens arrays," Appl. Opt. **41**, 2575–2585 (2002).
23. K. Tvingstedt, S. Dal Zilio, O. Inganäs, and M. Tormen, "Trapping light with micro lenses in thin film organic photovoltaic cells," Opt. Express **16**, 21608–21615 (2008).
24. V. Arrizón, U. Ruiz, R. Carrada, and L. A. González, "Pixelated phase computer holograms for the accurate encoding of scalar complex fields," J. Opt. Soc. Am. A **24**, 3500–3507 (2007).
25. V. Arrizón, G. Méndez, and D. Sánchez-de-La-Llave, "Accurate encoding of arbitrary complex fields with amplitude-only liquid crystal spatial light modulators," Opt. Express **13**, 7913–7927 (2005).
26. M. Agour, C. Falldorf, and C. Koyplow, "Digital pre-filtering approach to improve optically reconstructed wavefields in opto-electronic holograph," J. Opt. A **12**, 055401 (2010).
27. E. Lepera, C. Provenzano, P. Pagliusi, and G. Cipparrone, "Liquid crystal based polarization gratings for spectro-polarimetric applications," Mol. Cryst. Liq. Cryst. **558**, 109–119 (2012).
28. P. Pagliusi, E. Lepera, C. Provenzano, A. Mazzulla, and G. Cipparrone, "Polarization gratings allow for real-time and artifact-free circular dichroism measurements," Proc. SPIE **8069**, 806910 (2011).
29. C. Provenzano, P. Pagliusi, and G. Cipparrone, "Highly efficient liquid crystal based diffraction grating induced by polarization holograms at the aligning surfaces," Appl. Phys. Lett. **89**, 121105 (2006).